$$\overline{AlOH_2} \rightarrow \overline{AlOH^- + H^+} \quad (7)$$

Evidence for intracrystalline chain propagation is provided by the abundance of 10–50-Å ruthenium aggregates buried within the support particle and the rare occurrence of metal particles on external surfaces (cf. Figure 2). We believe the metal aggregates observed by electron microscopy are formed by migration of ruthenium atoms to defect sites in the clay particle. These defect sites may be formed by layer folding and the formation of interfaces between discrete clay layers, as illustrated in Figure 5. The presence of additional ruthenium, encapsulated within the galleries and too small (<10 Å) to be observed in our electron microscopy studies, is unlikely. Our preliminary H_2 chemisorption studies indicate that the Ru dispersion is <10%, as expected for 10–50-Å particles located in defect sites. Even with all the ruthenium contained as larger aggregates in defect sites, the terminal olefins formed by FT chain propagation would still be obliged to contact the highly acidic gallery surfaces in diffusing out of the particle.

Ruthenium as a FT catalyst has been supported on a number of different zeolties.[64-68] In most cases the hydrocarbon products are terminal olefins and normal paraffins. A notable exception is the hydrogen-exchange form of dealuminated zeolite Y. This highly acidic microporous support also affords high yields of isomerized FT hydrocarbons,[67,68] comparable to those observed here for Ru–APM. When ruthenium is introduced into the zeolite by ion exchange and subsequently reduced under hydrogen, metal aggregates as large as 20 Å are embedded within the crystals.[69,70] Thus, there are strong parallels between our alumina pillared clay and hydrogen-exchanged zeolite Y with regard to their intrinsic acidity and ability to support metal particles in intracrystalline environments.

Finally, we note that the high branching selectivity in the FT synthesis of hydrocarbons can have important practical advantages. For instance, the presence of branched isomers in the gasoline range (C_5–C_{12}) should provide high octane numbers. Also, branching should improve the viscosities of the higher molecular weight fractions used for diesel fuel and jet fuel and as lubricants. Thus, pillared clays are promising materials for the design of selective syn gas catalysts for future energy needs.

Acknowledgment. The support of this research by the National Science Foundation, Division of Materials Research (Grant DMR-8514154), and the Michigan State University Center for Fundamental Materials Research is gratefully acknowledged. Fellowship support for E.P.G. and E.G.R. was provided by Exxon Corp. and ICC International, respectively. We thank Dr. Michael Siskin (Exxon) and Dr. Paul Reid (ECC) for their support and helpful discussions.

Registry No. $Ru_3(CO)_{12}$, 15243-33-1; $Os_3(CO)_{12}$, 15696-40-9; $Ir_3(CO)_{12}$, 18827-81-1; $H_2Os_3(CO)_{12}$, 12560-48-4; $H_4Ru_4(CO)_{12}$, 34438-91-0; Os, 7440-04-2; Ru, 7440-18-8; Ir, 7439-88-5; montmorillonite, 1318-93-0.

(64) Chen, Y. W.; Wang, h. T.; Goodwin, J. G., Jr. *J. Catal.* **1983**, *83*, 415.
(65) Chen, Y. W.; Wang, H. T.; Goodwin, J. G., Jr. *J. Catal.* **1984**, *85*, 499.
(66) Nijs, N. H.; Jacobs, P. A. *J. Catal.* **1980**, *66*, 401.
(67) Tatsumi, T.; Shul, Y. G.; Sugivra, T.; Tominaga, H. *Appl. Catal.* **1986**, *21*, 119.
(68) King, D. L. *J. Catal.* **1978**, *51*, 386.
(69) Verdonck, J. J.; Jacobs, P. A.; Gent, M.; Poncelet, G. *J. Chem. Soc., Faraday Trans. 1* **1980**, *76*, 403.
(70) Gustafson, B. L.; Lunsford, J. H. *J. Catal.* **1982**, *74*, 393.

The Influence of Guest–Host Interactions on the Excited-State Properties of Dioxorhenium(V) Ions in Intracrystalline Environments of Complex-Layered Oxides

Mark D. Newsham, Emmanuel P. Giannelis, Thomas J. Pinnavaia,* and Daniel G. Nocera*

Contribution from the Department of Chemistry and the Center for Fundamental Materials Research, Michigan State University, East Lansing, Michigan 48824-1322.
Received October 16, 1987

Abstract: The excited-state properties of *trans*-dioxorhenium(V) ions immobilized in the intracrystalline environments of three complex-layered oxides (CLOs) have been examined. The layered silicate CLOs hectorite and fluorohectorite adsorb *trans*-$ReO_2(py)_4^+$ to their negatively charged interlayers by intercalative ion exchange to produce topotactic solids with gallery heights of 6.7 and 9.2 Å, respectively. A dioxorhenium CLO of complementary charge, prepared by the addition of NaOH to an aqueous solution containing $MgCl_2$:$AlCl_3$ (1:2 w/w) and *trans*-$ReO_2(CN)_4^{3-}$, incorporates the oxoanion between the positive layers of a hydrotalcite-like Mg/Al double hydroxide. Electronic absorption and vibrational spectra of these three CLO intercalates are characteristic of the dioxorhenium ions and are indicative of structurally unperturbed oxo complexes in the CLO intracrystalline environment. Despite structurally similar intercalated *trans*-ReO_2^+ cores, steady-state and time-resolved luminescence experiments reveal that the three CLO intercalates are quite distinct: solid $ReO_2(py)_4$–hectorite is highly emissive ($\lambda_{em,max}$ = 630 nm at 25 °C) and luminescence spectra display progressions in 900-cm^{-1} ($\nu_{a_{1g}}$(Re–O)) and 200-cm^{-1} ($\nu_{a_{1g}}$(Re–py)) modes similar to that of the native ion; $ReO_2(py)_4$–fluorohectorite exhibits broad and featureless emission ($\lambda_{em,max}$ = 685 nm at 25 °C) whose intensity is attenuated by a factor of 50 relative to the hectorite compound and, $ReO_2(CN)_4$–hydrotalcite does not luminesce. The luminescence decay curve of $ReO_2(py)_4$–hectorite displays multiexponential form with a major lifetime component of 13.0 μs and a minor lifetime component of 3.9 μs. In contrast, the emission decay of the fluorohectorite intercalate is uniexponential and fast (τ = 0.63 μs). The disparate excited-state properties of the three intercalates are attributed to specific guest–host interactions which mediate the reaction between the *trans*-ReO_2^+ core and water in the CLO interlayers.

Photochemical processes can significantly be modified with the intercalation of reactants within intracrystalline environments of zeolites,[1-4] layered phosphates,[5] and complex-layered oxides (CLOs).[6-10] Layered silicate clays (LSCs) and layered double

0002-7863/88/1510-3885$01.50/0

hydroxides (LDHs) are the CLO supports that have been used to mediate the physical and chemical properties of electronically excited guest molecules. Size and shape restrictions and specific chemical equilibria are known to mediate the pathways of thermal reactions in CLO galleries,[11] and similar intracrystalline effects can alter the reaction selectivities of electronically excited molecules.[12] The structure of LSCs consists of negatively charged, two-dimensional silicate layers which are separated by sheets of hydrated cations in the galleries, while LDHs are complementary structures to the LSCs in that the charge of the layers and gallery ions is reversed. Simple ion-exchange procedures permit a variety of cations and anions of virtually any size to be accommodated in the galleries of LSCs and LDHs, respectively. To date, inorganic photochemical studies have primarily centered on LSC and LDH intercalates of metal polypyridyl complexes.[6,8,9f,10] Principal themes that have emerged from consideration of the luminescence properties of these intercalates is that excited-state properties are generally preserved upon intercalation, and the photoactive ions are accessible for excited-state electron- and energy-transfer reactions. Specific effects of LSC and LDH host structures on the dynamics of excited-state processes, however, have been experimentally difficult to assess owing to the relative insensitivity of the excited-state properties of metal polypyridyl complexes to environmental effects. Consequently, the extent to which excited-state properties such as lifetime, energy, and geometry are perturbed by guest–host interactions in LSC and LDH intercalates has, for the most part, remained undefined.

In an effort to better understand guest–host interactions of photoactive CLOs, we decided to explore the spectroscopy and photophysics of high-valent transition-metal–oxo compounds in LSC and LDH galleries. The results of electronic absorption and emission studies have provided a detailed account of the electronic structure of metal–oxo compounds[13-22] and suggest that this class of photoreagents and, particularly, d^2 *trans*-dioxo species[21] are well-suited to probe the effect of LSC and LDH intracrystalline environments on excited-state properties. In particular, recent investigations of *trans*-dioxorhenium(V) complexes have demonstrated that the lowest energy ligand field transitions, which involve the promotion of an electron from the $b_{2g}(xy)$ orbital to the doubly degenerate Re–O π-antibonding $e_g(xz,yz)$ level, produce $^1E_g[(b_{2g})^1(e_g)^1]$ and $^3E_g[(b_{2g})^1(e_g)^1]$ states, the latter of which is highly emissive.[21,22] The excited-state lifetime and energy of the ^3E_g state is quite sensitive to the environment, and protic solvents efficiently quench the molecular luminescence. Along these lines, it is reasonable to expect that the extent of complex formation between the photoactive gallery ion and the interlayer water molecules of LSCs and LDHs, and hence the luminescence properties of the intercalates, will be extremely sensitive to the orientation and specific interaction of the *trans*-ReO_2^+ cores within the intracrystalline environment. Moreover, the ability to vary the charge of the dioxorhenium(V) complexes with the ancillary ligands in the equatorial coordination sites while maintaining the luminescent properties of the metal–oxo core allows for a comparative study of the effect of the anionic LSC and cationic LDH environments on the excited-state dynamics of structurally and electronically similar gallery ions to be undertaken. We report herein results of our spectroscopic and photophysical investigations of the LSC and LDH intercalates containing the *trans*-$ReO_2(py)_4^+$ (py = pyridine) and *trans*-$ReO_2(CN)_4^{3-}$ complexes, respectively, as well as our discovery that guest–host interactions can engender luminescence from dioxorhenium(V) species in highly protic environments.

Experimental Section

Materials and Synthesis. All chemicals were analytical reagent grade and were used as received. Rhenium–oxo compounds $[ReO_2(py)_4]I$,[23] $K_3[ReO_2(CN)_4]$,[24] and $[ReO_2(en)_2]Cl$[25] (en = ethylenediamine) were prepared as previously described.

Natural sodium hectorite (San Bernardino County, CA) was obtained in spray-dried form from the Source Clay Mineral Repository, University of Missouri. The mineral was suspended in water (1 wt%) and allowed to sediment to remove carbonate impurities. The clay fraction containing particles less than 2 μm was collected, saturated with Na^+ ions by the addition of sodium chloride, dialyzed, and freeze dried. The cation-exchange capacity of the hydrated mineral was 70 mequiv/100 g. Fluorohectorite is a synthetic product analogous to that described by Barrer.[26]

(1) (a) Turro, N. J. *Pure Appl. Chem.* **1986**, *58*, 1219–1228. (b) Turro, N. J.; Lei, X.-G.; Cheng, C.-C.; Corbin, D. R.; Abrams, L. *J. Am. Chem. Soc.* **1985**, *107*, 5824–5826. (c) Turro, N. J.; Cheng, C.-C.; Lei, X.-G.; Flanigen, E. M. *J. Am. Chem. Soc.* **1985**, *107*, 3739–3741. (d) Turro, N. J.; Wan, P. *J. Am. Chem. Soc.* **1985**, *107*, 678–682. (e) Turro, N. J.; Wan, P. *Tetrahedron Lett.* **1984**, *25*, 3655–3658.

(2) (a) Tanguay, J. F.; Suib, S. L. *Catal. Rev.* **1987**, *29*, 1–40. (b) Suib, S. L.; Carrado, K. A. *Inorg. Chem.* **1985**, *24*, 200–202. (c) Suib, S. L.; Kostapapas, A.; McMahon, K. C.; Baxter, J. C.; Winiecki, A. M. *Inorg. Chem.* **1985**, *24*, 858–863. (d) Suib, S. L.; Kostapapas, A.; Psaras, D. *J. Am. Chem. Soc.* **1984**, *106*, 1614–1620. (e) Suib, S. L.; Bordeianu, O. G.; McMahon, K. C.; Psaras, D. *ACS Symp. Ser.* **1982**, *177*, 225–238.

(3) (a) Camara, M. J.; Lunsford, J. H. *Inorg. Chem.* **1983**, *22*, 2498–2501. (b) Quayle, W. H.; Lunsford, J. H. *Inorg. Chem.* **1982**, *21*, 97–103. (c) DeWilde, W.; Peeters, G.; Lunsford, J. H. *J. Phys. Chem.* **1980**, *84*, 2306–2310.

(4) (a) Wilkinson, F.; Willsher, C. J.; Casal, H. L.; Johnston, L. J.; Scaiano, J. C. *Can. J. Chem.* **1986**, *64*, 539–544. (b) Casal, H. L.; Scaiano, J. C. *Can. J. Chem.* **1985**, *63*, 1308–1314. (c) Scaiano, J. C.; Casal, H. L.; Netto-Ferreira, J. C. *ACS Symp. Ser.* **1985**, *278*, 211–222. (d) Casal, H. L.; Scaiano, J. C. *Can. J. Chem.* **1984**, *62*, 628–629.

(5) (a) Verschoor, C. M.; Olken, M. M.; Ellis, A. B. *J. Less-Common Met.* **1986**, *126*, 221–226. (b) Verschoor, C. M.; Ellis, A. B. *Solid State Ionics* **1986**, *22*, 65–69. (c) Olken, M. M.; Verschoor, C. M.; Ellis, A. B. *Inorg. Chem.* **1986**, *25*, 80–82. (d) Olken, M. M.; Ellis, A. B. *J. Am. Chem. Soc.* **1984**, *106*, 7468–7471. (e) Olken, M. M.; Verschoor, C. M.; Ellis, A. B. *J. Lumin.* **1984**, 31–32, 552–554. (f) Olken, M. M.; Biagioni, R. N.; Ellis, A. B. *Inorg. Chem.* **1983**, *22*, 4128–4134.

(6) Giannelis, E. P.; Nocera, D. G.; Pinnavaia, T. J. *Inorg. Chem.* **1987**, *26*, 203–205.

(7) Suib, S. L.; Carrado, K. A. *Inorg. Chem.* **1985**, *24*, 863–867.

(8) Ghosh, P. K.; Bard, A. J. *J. Phys. Chem.* **1984**, *88*, 5519–5526.

(9) (a) Nakamura, T.; Thomas, J. K. *J. Phys. Chem.* **1986**, *90*, 641–644. (b) Nakamura, T.; Thomas, J. K. *Langmuir* **1985**, *1*, 568–573. (c) Kovar, L.; DellaGuardia, R.; Thomas, J. K. *J. Phys. Chem.* **1984**, *88*, 3595–3599. (d) DellaGuardia, R. A.; Thomas, J. K. *J. Phys. Chem.* **1984**, *88*, 964–970. (e) DellaGuardia, R. A.; Thomas, J. K. *J. Phys. Chem.* **1983**, *87*, 3550–3557. (f) DellaGuardia, R. A.; Thomas, J. K. *J. Phys. Chem.* **1983**, *87*, 990–998.

(10) (a) Nijs, H.; Fripiat, J. J.; Van Damme, H. *J. Phys. Chem.* **1983**, *87*, 1279–1282. (b) Nijs, H.; Cruz, M. I.; Fripiat, J. J.; Van Damme, H. *Nouv. J. Chim.* **1982**, *6*, 551–557. (c) Abdo, S.; Canesson, P.; Cruz, M.; Fripiat, J. J.; Van Damme, H. *J. Phys. Chem.* **1981**, *85*, 797–809. (d) Nijs, H.; Cruz, M.; Fripiat, J.; Van Damme, H. *J. Chem. Soc., Chem. Commun.* **1981**, 1026–1027.

(11) (a) Pinnavaia, T. J. *Science (Washington, D.C.)* **1983**, *220*, 365–371. (b) Thomas, J. M. In *Intercalation Chemistry*; Whittingham, M. S., Jacobson, A. J., Eds.; Academic Press: New York, 1982; pp 55–99. (c) Laszlo, P. *Science (Washington, D.C.)* **1987**, *235*, 1473–1477. (d) Ballantine, J. A. In *Chemical Reactions in Organic and Inorganic Constrained Systems*; Setton, R., Ed.; Reidel: Boston, 1986; pp 197–212. (e) Fripiat, J. J. *Clays Clay Miner.* **1986**, *34*, 501–506.

(12) Suib, S. L.; Tanguay, J. F.; Occelli, M. L. *J. Am. Chem. Soc.* **1986**, *108*, 6972–6977.

(13) (a) Ballhausen, C. J.; Gray, H. B. *Inorg. Chem.* **1962**, *1*, 111–122. (b) Gray, H. B.; Hare, C. R. *Inorg. Chem.* **1962**, *1*, 363–368. (c) Miskowski, V.; Gray, H. B.; Ballhausen, C. J. *Mol. Phys.* **1974**, *28*, 729–745. (d) Winkler, J. R.; Gray, H. B. *Comm. Inorg. Chem.* **1981**, *1*, 257–263.

(14) (a) Collison, D.; Gahan, B.; Garner, C. D.; Mabbs, F. E. *J. Chem. Soc., Dalton Trans.* **1980**, 667–674. (b) Hill, L. H.; Howlader, N. C.; Mabbs, F. E.; Hursthouse, M. B.; Malik, K. M. A. *J. Chem. Soc., Dalton Trans.* **1980**, 1475–1481.

(15) Sunil, K. K.; Rogers, M. T. *Inorg. Chem.* **1981**, *20*, 3283–3287.

(16) Rappé, A. K.; Goddard, W. A. *J. Am. Chem. Soc.* **1982**, *104*, 448–456.

(17) Antipas, A.; Buchler, J. W.; Gouterman, M.; Smith, P. D. *J. Am. Chem. Soc.* **1980**, *102*, 198–207.

(18) (a) Tatsumi, K.; Hoffmann, R. *Inorg. Chem.* **1980**, *19*, 2656–2658. (b) Tatsumi, K.; Hoffmann, R. *Inorg. Chem.* **1981**, *20*, 3771–3784.

(19) Hanson, L. K.; Chang, C. K.; Davis, M. S.; Fajer, J. *J. Am. Chem. Soc.* **1981**, *103*, 663–670.

(20) Loew, G. H.; Herman, Z. S. *J. Am. Chem. Soc.* **1980**, *102*, 6173–6174.

(21) Winkler, J. R.; Gray, H. B. *J. Am. Chem. Soc.* **1983**, *105*, 1373–1374.

(22) Winkler, J. R.; Gray, H. B. *Inorg. Chem.* **1985**, *24*, 346–355.

(23) Beard, J. H.; Casey, J.; Murmann, R. K. *Inorg. Chem.* **1965**, *4*, 797–803.

(24) Beard, J. H.; Calhoun, C.; Casey, J.; Murmann, R. K. *J. Am. Chem. Soc.* **1968**, *90*, 3389–3394.

(25) Murmann, R. K. *Inorg. Synth.* **1966**, *8*, 173–174.

The particle size of this LSC is $\gg 2$ μm, and its cation-exchange capacity is 190 mequiv/100 g.

The $ReO_2(py)_4$–LSC intercalates were prepared by using simple ion-exchange methods. In a typical experiment sodium–hectorite (0.1 g, 0.070 mequiv) in 10 mL of water was added with stirring to a solution of the rhenium oxocation complex (0.070 mequiv) dissolved in the minimum amount of acetone. The clay immediately flocculated and turned yellow upon contacting the metal complex solution. After a reaction time of 10 min, the product was collected by centrifugation, washed several times with acetone to remove physically adsorbed cluster, and air dried.

The $ReO_2(CN)_4$–LDH intercalate was most successfully prepared by coprecipitating the hydrotalcite in the presence of the complex anion. $K_3[ReO_2(CN)_4]$ (0.44 g, 1.0 mmol), $MgCl_2 \cdot 6H_2O$ (1.83 g, 9.0 mmol), and $AlCl_3 \cdot 6H_2O$ (0.73 g, 3.0 mmol) were dissolved in 100 mL of degassed water. The solution pH was adjusted to 10 with 1 N NaOH, and the suspension was refluxed for 24 h and aged at room temperature for 3 days. The resulting precipitate was collected by centrifugation, washed, and dried in air.

Instrumentation and Methods. Infrared spectra, taken on a Perkin Elmer 599, were recorded on KBr pellets containing the intercalated solids. Resonance Raman experiments were performed with a Spex 1401 double monochromator and associated Ramalog electronics. A Spectra Physics 165 argon ion laser was the excitation source and incident powers were 50–60 mW. All spectra were collected at a 90° scattering geometry from H_2O suspensions of the intercalate at room temperature.

Electronic absorption spectra were recorded on a Cary 17D spectrophotometer. Molar absorptivities were experimentally determined from suspensions of clay intercalates. Volumes of a standardized aqueous solution of the dioxorhenium(V) ion were added to aqueous suspensions of the clay to yield 15%-exchanged CLO intercalates. The absorbance of these solutions was measured and molar extinction coefficients were calculated assuming the suspensions were homogeneously dispersed. After all absorbance measurements, suspensions of the clay intercalates were centrifuged, and the absorption spectra of the supernatants were recorded to ensure complete intercalation of the rhenium complex.

Luminescence spectra were recorded on an instrument designed and constructed at Michigan State that has previously been described.[27] Spectra recorded at 9 K were on samples cooled with an Air Products CSA-202E cryogenic refrigeration system equipped with a DMX-1 vacuum shroud interface, DE-202 expander module, and a IRO2A air-cooled compressor. Solid samples were adhered to a copper block with copper grease (a mixture of fine copper filings and Apiezon H grease), and the block was mounted to the sample head of the DE-202. An iridium gasket between the copper block, and the DE-202 ensured good thermal conductivity. The temperature was varied with the resistive heating element of an APD-E digital indicator/controller and was monitored with an iron-doped gold-chromel thermocouple mounted at the end of the DE-202 expander module.

Emission lifetimes were acquired with a pulsed laser system built at Michigan State. The excitation source was a Quanta Ray DCR-1 Nd-YAG laser frequency doubled or tripled with a Quanta Ray HG-2 harmonic generator followed by a Quanta Ray PHS-1 prism harmonic separator to produce a respective 532- or 355-nm pulse of 8-ns (fwhm) duration at 2 Hz. Emitted light from the sample was collected at 90° to the excitation beam with a collimating lens (f/1.5) and then focussed by a second lens (f/7) through a Schott OG-570 color filter onto the entrance slit of a GCA/McPherson EU-700 scanning monochromator. Luminescence was monitored at wavelengths corresponding to the emission maximum of suspensions or solids of the CLO intercalates and detected by a Hamamatsu R1104 photomultiplier tube. The signal from the PMT was passed through a home-built current sensitive preamplifier, employing a LeCroy VV100B fast pulse linear amplifier, to the 50-Ω impedance input of a LeCroy 6102 dual amplifier/trigger. The output of the amplifier was passed into a LeCroy TR8828B transient recorder, and the digitized signal was stored in two LeCroy MM8104 memory modules arranged in a series configuration. The amplifier, digitizer, memory modules, and a LeCroy 8901 GPIB interface were housed in a LeCroy 8013A minicrate. Data, acquired and processed by a Zenith-151-52 minicomputer equipped with a 10 megabyte hard disc, were typically averaged over 1000 laser pulses. Uniexponential decay curves were fit by using standard least-squares linear regression statistics. Plots of log (intensity) versus time were linear over at least 3 lifetimes. Multiexponential decay curves were fit to the equation $y = ae^{-t/\tau_1} + be^{-t/\tau_2}$ by using the Kinfit[28] general nonlinear curve-fitting program where τ_1 and τ_2 are the excited-state lifetimes. Convergence of the fit, monitored by the sum of the squares of the residuals, yielded values for a, b, τ_1, and τ_2.

The reaction of electronically excited dioxorhenium(V) ions with proton donors was studied by using the Stern–Volmer quenching method.[29] Luminescence quenching was monitored with time-resolved luminescence spectroscopy. Samples were prepared by adding dimethylformamide (DMF) solutions of the *trans*-dioxorhenium(V) ion to DMF suspensions of the CLO. Aliquots of H_2O were delivered to CLO suspensions of the intercalate with a 100-μL Hamilton syringe. All lifetime measurements were performed on solutions thoroughly degassed with argon.

Table I. Idealized Structural Formulas of Complex-Layered Oxides

complex-layered oxide	formula
hectorite	$Na_{0.67}[Mg_{5.33}Li_{0.67}](Si_{8.00})O_{20}(OH,F)_4$[a]
fluorohectorite	$Li_{1.6}[Mg_{4.4}Li_{1.6}](Si_{8.00})O_{20}F_4$
hydrotalcite	$[Mg_{0.75}Al_{0.25}(OH)_2]Cl_{0.25} \cdot H_2O$[b]

[a] In this CLO some framework hydroxyls are replaced by fluoride. [b] Synthetic hydrotalcites are characterized by the generalized formula $[M^{II}_{1-x}M^{III}_x(OH)_2]A^{n-}_{x/n} \cdot yH_2O$, where $x = 0.20$–0.33, A^{n-} is the gallery anion, and M^{II} and M^{III} are di- and tripositive ions. In the mineral hydrotalcite $M^{II} = Mg^{2+}$, $M^{III} = Al^{3+}$ and $A^{n-} = CO_3^{2-}$.

Results

Synthesis and Characterization. The structural formulas of the CLO host structures used in our studies are presented in Table I. The LSCs are 2:1 phyllosilicates whose structures consist of elementary layers composed of an octahedral sheet of oxygen and hydroxyl ions coordinating Mg^{2+} or Li^+ ions sandwiched between two tetrahedral sheets coordinating Si^{4+} ions.[30] A net negative charge on these elementary layers, resulting from the isomorphic substitution of Li^+ for Mg^{2+} ions in the octahedral sites is balanced by a sheet of hydrated sodium or lithium ions. As indicated by the formulas listed in Table I, fluorohectorite is distinguished from hectorite simply by increased Li^+ substitution in the octahedral layer. The increased layer charge of fluorohectorite is manifested in a concomitant increase in the interlayer cation concentration. In contrast to the properties of LSCs, the reversed layer and gallery charges of the LDHs results from the replacement of divalent cations by trivalent cations in brucite-like (i.e., $Mg(OH)_2$-like) octahedral sheets. Table I lists the chemical composition of a synthetic hydrotalcite, which is characterized by substitution of Al^{3+} for Mg^{2+} in the octahedral sites.[31-33] The LDH host structure is typically prepared by precipitating the double hydroxide from an aqueous NaOH solution containing the aluminum and magnesium chloride salts.

The ion-exchange properties of LSCs and LDHs suggested that the appropriately charged dioxorhenium(V) ions would be incorporated readily into the galleries of the host structures. Addition of aqueous suspensions of Na-exchanged hectorite and fluorohectorite LSCs and Cl-exchanged hydrotalcite LDH to aqueous solutions of $ReO_2(py)_4^+$ and $ReO_2(CN)_4^{3-}$, respectively, yielded yellow solids. All spectroscopic and photophysical studies employed samples with loadings of the metal–oxo complex corresponding to 15% of the ion-exchange capacity of the CLO; chemical compositions of the exchanged CLOs were confirmed by spectrophotometric analysis. The IR spectra of these solids, reproduced in Figure 1, indicate that the dioxorhenium(V) complexes are immobilized on the CLO supports. The $ReO_2(py)_4$–LSC solids exhibit an IR spectrum consisting of the superposition of the metal–oxo cation spectrum on that of the LSC support. Bands attributable to ring stretching vibrations of the pyridine at 1490 and 1502 cm^{-1} are clearly apparent in the KBr pellet spectra of the $ReO_2(py)_4$–LSC solids. Similarly, the C–N

(26) Barrer, R. M.; Jones, D. L. *J. Chem. Soc. A* **1970**, 1531–1537.
(27) Mussell, R. D.; Nocera, D. G. *J. Am. Chem. Soc.* **1988**, *110*, 2764–2772.
(28) Dye, J. L.; Nicely, V. A. *J. Chem. Ed.* **1971**, *48*, 443–448.
(29) Balzani, V.; Moggi, L.; Manfrin, M. F.; Bolletta, F. *Coord. Chem. Rev.* **1975**, *15*, 321–433.
(30) Bailey, S. W. In *Crystal Structures of Clay Minerals and Their X-ray Identification*; Brindley, G. W., Brown, G., Eds.; Mineralogical Society: Britain, 1980; Chapter 1.
(31) Gastuche, M. C.; Brown, G.; Mortland, M. M. *Clay Miner.* **1967**, *7*, 177–192.
(32) Miyata, S. *Clays Clay Miner.* **1980**, *28*, 50–56.
(33) Taylor, R. M. *Clay Miner.* **1984**, *19*, 591–603.

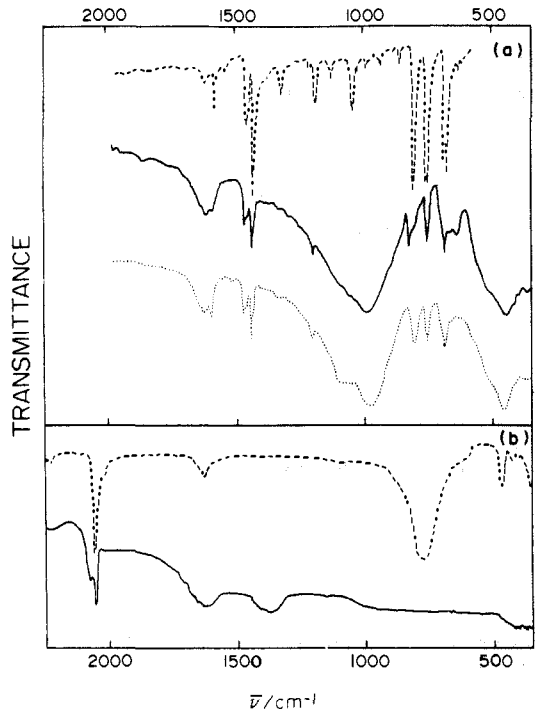

Figure 1. Infrared spectra on KBr pellets of the following: (a) (---) $[ReO_2(py)_4]I$; (—)$ReO_2(py)_4$–hectorite; (···) $ReO_2(py)_4$–fluorohectorite; (b) (---) $K_3[ReO_2(CN)_4]$; (—) $ReO_2(CN)_4$–hydrotalcite.

stretching vibrations of $ReO_2(CN)_4^{3-}$ adsorbed to LDH are little shifted relative to that observed for KBr pellet spectra of the native anion. Although the infrared active O–Re–O vibrations are obscured by absorptions of the metal–oxo lattice vibrations of the aluminosilicate and double hydroxide host structures, Raman spectra obtained by using excitation frequencies coincident with the $^1E_g \leftarrow {}^1A_{1g}$ absorption leads to a significant enhancement of the Raman peaks associated with metal–oxygen vibrations. A prominent band corresponding to the totally symmetric O–Re–O stretching vibration is observed at 916 and 919 cm^{-1} for the $ReO_2(py)_4$–hectorite and $ReO_2(py)_4$–fluorohectorite adsorbates, respectively. The energy of the metal–oxygen vibrations is only marginally shifted upon CLO immobilization ($\nu_{a_{1g}}$(Re–O) = 916 cm^{-1} for $ReO_2(py)_4^+$ in H_2O at 25 °C), and this result in conjunction with those from infrared spectroscopy reveals minor structural distortions, if any, of the bound complexes.

That the dioxorhenium(V) ions indeed occupy the LSC and LDH galleries is confirmed by the X-ray patterns of the reacted solids (see Figure 2). Basal spacings of the three layered products clearly reveal an expansion of the gallery upon adsorption of the dioxorhenium(V) complex. If we account for the van der Waals thickness of the LSC and LDH layers (d_{layer}(hectorite and fluorohectorite) = 9.5 Å; d_{layer}(hydrotalcite) = 4.8 Å), the 00*l* reflections for $ReO_2(py)_4$–hectorite, $ReO_2(py)_4$–fluorohectorite, and $ReO_2(CN)_4$–hydrotalcite correspond to gallery heights of 6.7, 9.0, and 4.3 Å, respectively. It is clearly apparent from these results that the dioxorhenium(V) ions do not reside in the CLO galleries with similar molecular orientations (vide infra). As typically observed in CLO intercalation chemistry, the relatively low order of 00*l* reflections for the three solids is indicative of interstratified intercalation of the *trans*-dioxorhenium(V) complexes.

Electronic Absorption and Emission Spectroscopy. The room temperature electronic absorption spectra of $ReO_2(py)_4$–hectorite and $ReO_2(py)_4$–fluorohectorite are reproduced in Figure 3a. The absorption profiles of these $ReO_2(py)_4^+$ intercalates are similar at wavelengths longer than 300 nm being characterized by a single intense absorption band between 350 and 400 nm and a less intense shoulder on the low-energy side. The shoulder is energetically coincident with the $^1E_g \leftarrow {}^1A_{1g}$ transition of $ReO_2(py)_4^+$ at 420 nm. Conversely, the 320-nm band shifts to lower energy upon intercalation of the complex. Disparate absorption cross sections and slightly different energies of this band for the hectorite (λ_{max} = 377 nm; ϵ = 29 700 M^{-1} cm^{-1}) and fluorohectorite intercalates (λ_{max} = 347 nm; ϵ = 13 100 M^{-1} cm^{-1}) suggest some type of perturbation of the electronic structure of the *trans*-ReO_2^+ core by the negatively charged silicate layers. Spectroscopic evidence implies that the 320-nm band of the native complex arises from either an $a_{1g}(z^2) \leftarrow b_{2g}(xy)$ transition or oxygen LMCT. Our data are consistent with the latter assignment because the LMCT should energetically be stabilized by the proximity of the oxygens of the *trans*-ReO_2^+ core to the negative silicate layers. The physical significance of the intensity variation of this transition

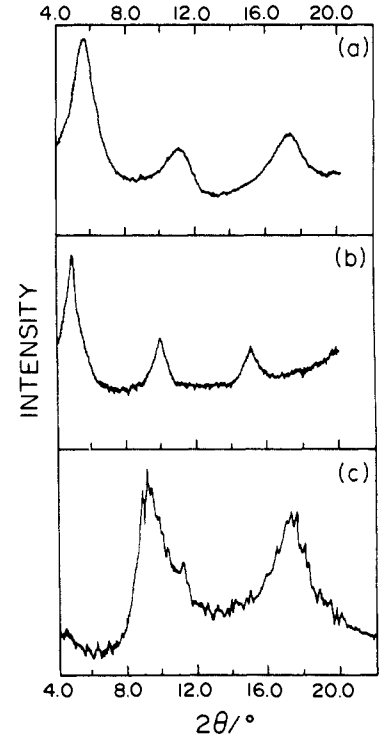

Figure 2. X-ray patterns of the three CLO intercalates: (a) $ReO_2(py)_4$–hectorite; (b) $ReO_2(py)_4$–fluorohectorite; (c) $ReO_2(CN)_4$–hydrotalcite.

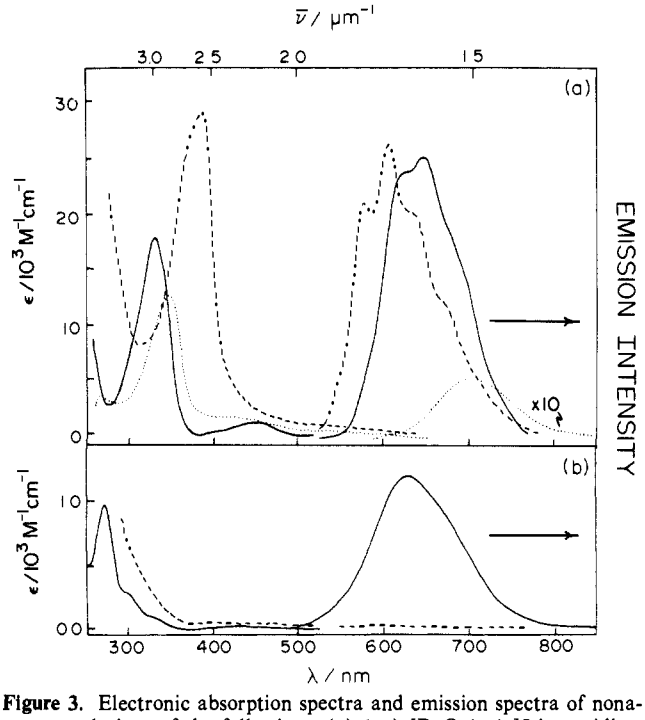

Figure 3. Electronic absorption spectra and emission spectra of nonaqueous solutions of the following: (a) (—) $[ReO_2(py)_4]I$ in pyridine; (---) $ReO_2(py)_4$–hectorite; (···) $ReO_2(py)_4$–fluorohectorite; (b) (—) $K_3[ReO_2(CN)_4]$ in DMF; (---) $ReO_2(CN)_4$–hydrotalcite.

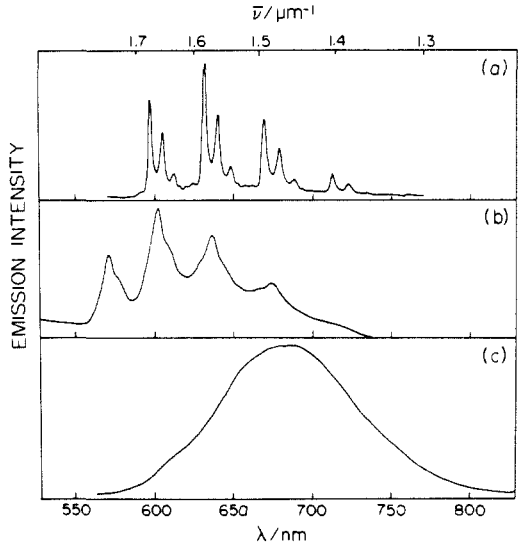

Figure 4. Low-temperature (9 K) emission spectra of solid: (a) $[ReO_2(py)_4]I$; (b) $ReO_2(py)_4$–hectorite; (c) $ReO_2(py)_4$–fluorohectorite.

presently remains unresolved.[34]

The LSC intercalates luminesce at room temperature with blue and near UV excitation. The red emission observed from these solids is characteristic of $ReO_2(py)_4^+$. The uncorrected emission spectra for $ReO_2(py)_4^+$ in deaerated pyridine, and aqueous suspensions of the hectorite and fluorohectorite intercalates are reproduced in Figure 3a. Emission spectra of the intercalated solids are independent of the excitation wavelength over the range of 313–436 nm and are insensitive to the loading of the oxocation. The emission maximum of the fluorohectorite intercalate is 685 nm, and the emission band is broad and featureless. In contrast, luminescence from $ReO_2(py)_4$–hectorite is shifted to the blue ($\lambda_{em,max}$ = 630 nm), and vibrational fine structure can be resolved. As observed from Figure 3a, the luminescence properties of the hectorite intercalate as opposed to the fluorohectorite intercalate more closely resemble that of the native $ReO_2(py)_4^+$ ion. Relative quantum yield measurements of aqueous suspensions of the LSC intercalates reveal that the luminescence intensity of $ReO_2(py)_4^+$ in fluorohectorite is 50 times less than that in hectorite.

Comparisons between the emission of $ReO_2(py)_4^+$ and $ReO_2(py)_4$–LSC intercalates are more readily accomplished at low temperature. Electronic emission spectra of $ReO_2(py)_4I$, $ReO_2(py)_4$–hectorite, and $ReO_2(py)_4$–fluorohectorite at 9 K are shown in Figure 4. While the emission band of the fluorohectorite intercalate remains featureless, the emission band of the hectorite intercalate consists of a distinct progression of 900 cm^{-1} subdivided by a less pronounced progression of 200 cm^{-1}. Similar progressions in 900- and 210-cm^{-1} modes are observed in the luminescence spectrum of crystalline $ReO_2(py)_4I$ at 9 K, and isotopic labeling studies have shown that these modes correspond to the symmetric rhenium–oxygen and rhenium–pyridine stretching vibrations, respectively.[22]

Electronic absorption and emission spectra of the $ReO_2(CN)_4$–LDH (Figure 3b) are much less informative than those of the $ReO_2(py)_4$–LSC intercalate compounds. The pale yellow color of the LDH intercalate arises from the absorption tail between 300 and 350 nm. However, the maximum of the ultraviolet peak responsible for this absorbance cannot be recorded due to significant scattering of light at wavelengths shorter than 300 nm. Additionally, the low loadings of the LDH galleries with $ReO_2(CN)_4^{3-}$ precluded observation of the weak $^1E_g \leftarrow {}^1A_{1g}$ transition. In contrast to the $ReO_2(py)_4$–LSC compounds, no luminescence (λ_{exc} = 365, 405, and 436 nm) is detected from $ReO_2(CN)_4$–LDH over the temperature range of 9–300 K.

(34) Similar intensity variations have been observed in the absorption spectra of other CLO intercalates.[6,8,37] The factors responsible for these intensity variations have also not been identified.

Table II. Solid, Solution, and Intercalate Luminescence Lifetimes of the $ReO_2(py)_4^+$ Ion[a]

medium	a	τ_1 (μs)	b	τ_2 (μs)
iodide salt[b]	1.00	33.0		
dimethylformamide[b]	1.00	9.6		
hectorite	0.37	3.9	0.63	13.0
hectorite/H_2O[c]	0.41	1.9	0.59	11.0
hectorite/D_2O[d]	0.43	3.1	0.57	12.0
fluorohectorite[b]	>0.97	0.63		
fluorohectorite/H_2O[b,c]	>0.99	0.35		
fluorohectorite/D_2O[d]	0.86	1.2	0.14	2.8

[a] Luminescence decay curves were fit to the multiexponential equation $y = ae^{-t/\tau_1} + be^{-t/\tau_2}$ where a and b represent the fractions of total emission decay described by the short-lifetime component τ_1 and long-lifetime component τ_2, respectively. [b] System exhibits uniexponential emission decay kinetics. [c] One wt% H_2O suspension of a 15%-exchanged LSC. [d] One wt% D_2O suspension of a 15%-exchanged LSC.

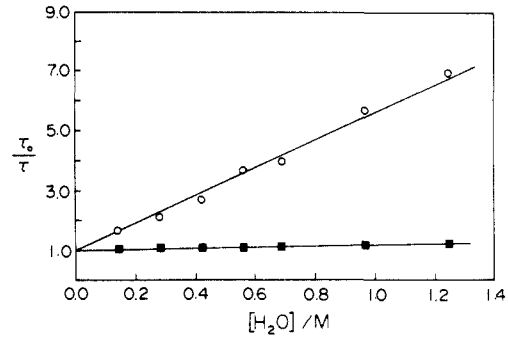

Figure 5. Stern–Volmer plot of the long lifetime component of $ReO_2(py)_4$–hectorite in DMF (■) with H_2O as the quencher, and $ReO_2(py)_4^+$ in DMF (○) with H_2O as the quencher.

Further insight into the excited-state properties of dioxorhenium(V) ions in CLO intracrystalline environments is provided by time-resolved luminescence measurements. Emission lifetimes of solids and suspensions of hectorite and fluorohectorite are listed in Table II; for purposes of comparison, the lifetimes of $ReO_2(py)_4^+$ as the iodide salt and in DMF solution are also included. For the latter two systems, the measured decay rates are in excellent agreement with previously reported lifetimes of solids and solutions of the $ReO_2(py)_4^+$ ion.[22] The luminescence decay of $ReO_2(py)_4^+$ in hectorite exhibits multiexponential behavior and can be fit reasonably well with a biexponential rate law with a = 0.37, τ_1 = 3.9 μs, b = 0.63, and τ_2 = 13.0 μs where a and b are the fraction of molecules with luminescence decays τ_1 and τ_2, respectively. The lifetime of the major component of the luminescence decay is comparable to that for the ion in homogeneous solution and remains relatively constant when $ReO_2(py)_4$–hectorite is suspended in H_2O and D_2O solutions. The short lifetime component of the decay curve, however, is quite sensitive to the nature of the solvent as evidenced by reduction of the lifetime by a factor of 2 when the intercalate is suspended in H_2O. Even more significant is the fact that this short lifetime component exhibits a distinct increase when $ReO_2(py)_4$–hectorite is suspended in D_2O. Interestingly, $ReO_2(py)_4^+$ residing in fluorohectorite galleries shows a short, predominantly single-exponential decay, and the trend of the excited-state lifetime on medium (e.g., solid, H_2O, D_2O) is parallel to that observed for the short lifetime component of the hectorite intercalate. Although the perturbation of the luminescence from $ReO_2(py)_4^+$ ion by H_2O and D_2O in CLO environments is expected in view of the extreme sensitivity of dioxorhenium(V) excited states toward proton donors,[22] the relative insensitivity of a significant fraction of $ReO_2(py)_4^+$ ions residing in the hectorite galleries to interstitial water is a surprising and unforseen result.

In order to quantitate this result we investigated the H_2O quenching of the luminescence from DMF suspensions of $ReO_2(py)_4$–hectorite by the Stern–Volmer method. A plot of the ratio of the long lifetime component of the $ReO_2(py)_4$–hectorite luminescence decay in the absence of H_2O to that in the presence

Table III. Emission Lifetime of $ReO_2(py)_4$-Hectorite Containing Co-Intercalated $ReO_2(en)_2^+$ Ions

$ReO_2(py)_4^+$/ $ReO_2(en)_2^+$ [a]	a[b]	τ_1[b] (μs)	b[b]	τ_2[b] (μs)
100:0	0.41	1.9	0.59	11.0
50:50	0.44	2.6	0.56	11.0
10:90	0.45	2.4	0.55	10.0

[a] Hectorite intercalate with 15% of the exchange capacity replaced by $ReO_2(py)_4^+$ and $ReO_2(en)_2^+$ ions in the given molar ratios. [b] Defined in the footnote of Table II.

of H_2O is shown in Figure 5; a Stern–Volmer plot obtained for $ReO_2(py)_4^+$ in DMF with H_2O as the quencher is also illustrated. Consistent with the Stern–Volmer equation, τ_0/τ varies linearly with the concentration of H_2O for the two systems. The Stern–Volmer constant for the luminescence quenching of $ReO_2(py)_4^+$ in homogeneous solution is 2 orders of magnitude greater than that of the ion incorporated in hectorite galleries.[35]

Discussion

The excited-state properties of dioxorhenium(V) ions exhibit a pronounced dependence on the CLO interlayer environments. We observe from time-resolved emission and steady-state luminescence experiments that the behavior of intercalated dioxorhenium(V) ions can be classified into three distinct categories: (i) the luminescent hectorite intercalate is largely unperturbed, and excited-state decay channels are similar to those of the dioxorhenium(V) ion in aprotic solution; (ii) emission from the ion in the fluorohectorite intercalate is significantly attenuated in intensity, and a corresponding decrease in the emission lifetime is observed; and (iii) no luminescence is detected from the dioxorhenium(V) core intercalated in LDH. These discrepancies in the luminescence properties of the structurally and electronically related rhenium–oxo complexes in CLO environments are significant and suggest unique and specific lifetime-limiting processes for the three CLO systems.

Luminescence quenching of photoactive ions in CLO interlayer environments has previously been attributed to either the presence of impurity ions isomorphically substituted into the octahedral sites in the layers[36,37] or efficient excited-state self-quenching processes promoted by the high local concentration of ions within the interlayer galleries.[8] However, several pieces of evidence suggest that neither of these two quenching mechanisms are operative in the dioxorhenium(V) CLO intercalate systems. First, quenching by impurity ions is precluded by the virtual absence of transition-metal ions (e.g., Fe^{3+}, Cr^{3+}) in the octahedral sites of the LSC and LDH host structures. Indeed, the synthetic hydrotalcite intercalate from which no emission is detected has only Al^{3+} and Mg^{2+} ions composing the sheet structure; and for the hectorite and fluorohectorite intercalate compounds, the concentration of cations other than Mg^{2+} or Li^+ is less than 0.1%. Second, luminescence decay kinetics of all the intercalates investigated do not exhibit a dependence on the presence of the nonemissive *trans*-$ReO_2(en)_2^+$ ions in the gallery.[38] The data presented in Table III for the hectorite intercalate are exemplary. If the intercalate was exhibiting self-quenching, then the emission decay time should become longer as the concentration of the nonemissive co-intercalate is increased owing to an increase in the center-to-center distance between lumophores in the gallery.[39] Of course, this conclusion is predicated on the tacit assumption that the $ReO_2(py)_4^+$ and $ReO_2(en)_2^+$ ions do not segregate in the CLO galleries. Considering the similar charges, sizes, and structures of these two oxocations, we believe our assumption is a reasonable one. Finally, the short lifetime component of the hectorite intercalate and the fluorohectorite intercalate exhibits a pronounced deuterium isotope effect which parallels that observed for the ion in nonaqueous solution. This result clearly demonstrates that the quenching decay channels of the intercalated ions are intimately related to the presence of proton donors in the interlayer region and suggests that the unique emission behavior of the three CLO systems is engendered by different guest–host interactions.

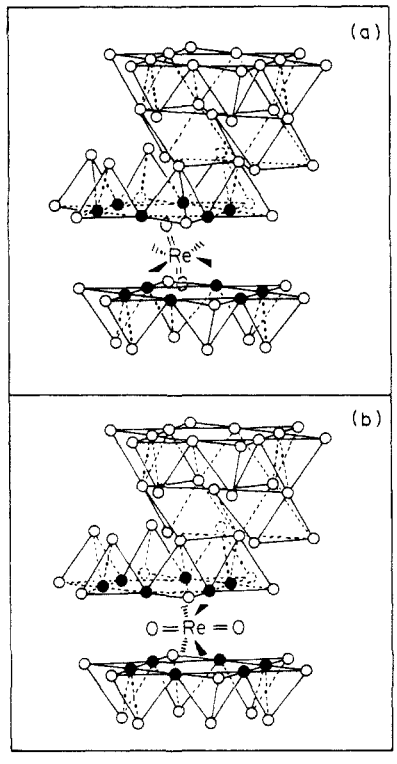

Figure 6. Proposed orientations of the *trans*-dioxorhenium(V) core in (a) hectorite and (b) fluorohectorite. The circles represent the idealized geometry for the oxygen framework of the LSC galleries. The oxygens comprising a hexagonal cavity of the CLO floor and ceiling are indicated by black circles.

The *d*-spacing of the three intercalate compounds offers additional evidence for the dioxorhenium(V) complexes occupying unique sites in the CLO interlayer environments. We first consider the $ReO_2(py)_4$–hectorite compound. A *d*-spacing of 6.7 Å is consistent with the guest complex assuming an orientation with the O–Re–O axis perpendicular to the layers of the host structure.[40] Interestingly, an average charge density of 80 Å^2 per unit negative charge on the aluminosilicate layer is calculated from

(35) The experimental manifestations of this result are quite striking. Aqueous solutions of $ReO_2(py)_4^+$ yield no luminescence upon visible or ultraviolet irradiation ($\lambda < 450$ nm). However, with the addition of powdered hectorite to the solution, red luminescence of $ReO_2(py)_4^+$ is observed almost immediately and grows in intensity as the ion-exchange reaction proceeds to completion (~10 min for a 1 wt% suspension of hectorite).

(36) (a) Habti, A.; Keravis, D.; Levitz, P.; Van Damme, H. *J. Chem. Soc., Faraday Trans. 2* **1984**, *80*, 67–83. (b) Bergaya, F.; Van Damme, H. *J. Chem. Soc., Faraday Trans. 2* **1983**, *79*, 505–518.

(37) Schoonheydt, R. A.; De Pauw, P.; Vliers, D.; De Schrijver, F. C. *J. Phys. Chem.* **1984**, *88*, 5113–5118.

(38) Despite the apparent electronic similarities of the $ReO_2(en)_2^+$ ion with that of the pyridine and cyanide analogues, the complex does not luminesce.[22] It has been suggested that the N–H vibrations of the ethylenediamine ligands provide efficient nonradiative decay channels to the ground electronic state. Stern–Volmer experiments show that $ReO_2(en)_2^+$ does not quench $ReO_2(py)_4^+$ luminescence.

(39) (a) Self-quenching can occur via dipole–dipole (Förster)[39b,c] or collisionally induced (Dexter)[39d] energy transfer. Either mechanism yields a larger quenching rate constant as the distance between the donor and acceptor molecules decreases. The Förster mechanism is a Coulombic interaction with $k_{et} \propto 1/R_{DA}^6$ (R_{DA} is the distance between donor and acceptor) and the Dexter mechanism depends on an exchange interaction between donor and acceptor with $k_{et} \propto \exp(-2R_{DA}/L)$ (L is the van der Waals radii of D and A). (b) Förster, T. *Disc. Faraday Soc.* **1959**, *27*, 7–17. (c) Zemel, H.; Hoffman, B. M. *J. Am. Chem. Soc.* **1981**, *103*, 1192–1201. (d) Dexter, D. L. *J. Chem. Phys.* **1953**, *21*, 836–850.

(40) (a) Average dimensions were calculated from crystallographic data for $[ReO_2(py)_4]Cl{\cdot}2H_2O$[40b] and $K_3[ReO_2(CN)_4]$[40c] and by using the van der Waals radii of the terminal atoms. For $ReO_2(py)_4^+$, the calculated lengths of the C_4 (O–Re–O), C_3 (for pseudooctahedral complex), and C_2'' axes (bisecting the pyridine–rhenium–pyridine equatorial axes) are 6.32, 5.44, and 9.43 Å, respectively. The calculated lengths of the C_4, C_3, and C_2'' axes are 6.36, 4.66, and 6.84 Å, respectively, for $ReO_2(CN)_4^{3-}$. (b) Calvo, C.; Krishnamachari, N.; Lock, C. J. L. *J. Cryst. Mol. Struct.* **1971**, *1*, 161–172. (c) Murmann, R. K.; Schlemper, E. O. *Inorg. Chem.* **1971**, *10*, 2352–2354.

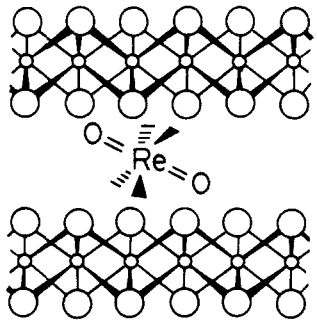

Figure 7. Proposed orientation of the *trans*-dioxorhenium(V) core in an idealized LDH gallery. The hydroxyl oxygens composing the LDH are represented by large circles and the metal ions by the smaller circles.

the unit cell dimensions of hectorite. When one considers that the cross-sectional area of the univalent oxocation situated along its C_4 axis is 89 Å^2, the $ReO_2(py)_4^+$ ion resides in the hectorite gallery with the orientation which most effectively counterbalances the layer charge. A parallel charge effect governs the intercalative reaction of fluorohectorite, but a higher charge density (27 Å^2/unit charge) for this CLO precludes intercalation of the oxocation along its C_4 axis. Alternatively, positioned on the C_2'' axis (bisecting the pyridine–rhenium–pyridine equatorial axes), the oxocation's cross-sectional area of 30 Å^2 is compatible with the layer charge density of fluorohectorite. The molecular dimension of 9.43 Å for the $ReO_2(py)_4^+$ ion along its C_2'' axis accounts nicely for the observed *d*-spacing of the fluorohectorite intercalate. In contrast to the LSC intercalates, the observed *d*-spacing of the LDH intercalate is in accordance with the effective C_3 axis of the pseudooctahedral $ReO_2(CN)_4^{3-}$ complex aligned normal to the host layers. Previous studies of hydrotalcites have demonstrated that the preferred orientation of intercalated anions either (i) maximizes the hydrogen-bonding interactions of the protons of the hydroxide layers with the guest species and/or (ii) minimizes the charge separation distance between the positive layers and gallery anions.[41] Both of these criteria are fulfilled by the observed orientation of the $ReO_2(CN)_4^{3-}$ anion. In view of these X-ray diffraction results in conjunction with the different luminescence properties of the three CLO intercalates, an intriguing issue is whether the unique orientations of the dioxorhenium(V) ions in the galleries can give rise to the disparate photophysical properties.

We address this question by considering the structures of the CLOs. The "ceiling" and "floor" of the LSC galleries are composed of basal planes of SiO_4 tetrahedra. An idealized geometry for the oxygen framework of LSC galleries is illustrated in Figure 6. The basal oxygens comprising SiO_4 tetrahedra are linked with neighboring tetrahedra to form hexagonal cavities of appreciable dimension (diametrically opposed vertices of the hexagon are separated by 5.28 Å). We propose that $ReO_2(py)_4^+$ in hectorite, lying on its C_4 axis, traverses the gallery with oxygens "keyed" into the hexagonal cavities of the CLO layers as shown in Figure 6a. This model accounts for the photophysical properties of the hectorite intercalate. In a keyed configuration, access of the hydroxyl protons of interlayer water molecules to the oxygens of the *trans*-ReO_2^+ core is inhibited, and quenching of $ReO_2(py)_4^+$ luminescence will be precluded. In accordance with our results for the long lifetime component of the emission decay of the hectorite intercalate, guest ions keyed into CLO layers are not expected to exhibit a deuterium isotope effect and will retain the long-lived, highly emissive excited-state properties characteristic of $ReO_2(py)_4^+$ ions in the solid state and nonaqueous solution. Additionally, if our proposed model is correct, then $ReO_2(py)_4^+$ ions which are not keyed into CLO layers should efficiently be quenched by interlayer H_2O. This is observed for the fluorohectorite intercalate. Indeed, our original motivation for investigating fluorohectorite was that this CLO provided us with the easiest route to rotating the oxygens of the *trans*-ReO_2^+ core away from the layers without altering the structural integrity of the LSC gallery. By assuming an orientation with the O–Re–O axis parallel to the fluorohectorite layers, as depicted in Figure 6b, the oxo core of the $ReO_2(py)_4^+$ ion is clearly accessible to water in the interlayer environment and, hence, the emission lifetime and intensity are significantly attenuated. The single exponential decay kinetics imply a predominantly uniform orientation of the $ReO_2(py)_4^+$ ions in the fluorohectorite gallery.

Along these lines our observation that the luminescence of a fraction of $ReO_2(py)_4^+$ ions incorporated in hectorite is quenched, giving rise to the short lifetime component of the emission decay profile, is consistent with incomplete keying of all the $ReO_2(py)_4^+$ ions in the interlayer environment. The quenchable ions may be aligned along their C_4 axis but with only one oxygen keyed into the CLO interlayer, or they may be in an orientation similar to that observed in the fluorohectorite intercalate. Although we presently cannot distinguish between these two limiting orientations, we are inclined to favor the former because we would expect ions with similar orientations in hectorite and fluorohectorite galleries to exhibit similar decay kinetics. Comparison of the data for the short lifetime component of hectorite and that of fluorohectorite shows that this is not the case.

Our inability to detect luminescence from $ReO_2(CN)_4$–LDH can now easily be understood within the context of the LSC results. As illustrated in Figure 7, the LDH gallery is bound by a cubic closed packed hydroxide sheet, and there are no cavities in which the rhenium–oxo core can key. Conversely, the oxygens of the *trans*-ReO_2^+ core are probably hydrogen bonded directly to the hydroxide layer. Because proton-donating solvents efficiently quench dioxorhenium(V) excited states by presumed hydrogen-bonding interactions,[22] the nonradiative decay rates of electronically excited $ReO_2(CN)_4^{3-}$ ions in LDH are expected to be exceedingly fast.

Thus, specific guest–host interactions in CLO intercalates can significantly mediate the excited-state properties of transition-metal complexes. By controlling subtle charge balancing effects between host and guest structures, highly emissive long-lived excited states can be preserved in reactive environments. We believe that our observations are completely general and can be extended to include many other metal–oxo compounds in CLO environments. The ability to use the CLO as a template to specifically align immobilized photoactive reagents in a gallery which can be accessed by a variety of reactants provides the opportunity to explore, and perhaps exploit, the effects of orientation on excited-state chemical reaction pathways.

Acknowledgment. The support of this work by the National Science Foundation through Grants CHE-8705871 (D.G.N.) and DMR-8514154 (T.J.P.) and the Michigan State University Center for Fundamental Materials Research is acknowledged. D.G.N. also gratefully acknowledges the Presidential Young Investigator Program and matching funds from the Exxon Education Foundation.

Registry No. $MgCl_2$, 7786-30-3; $AlCl_3$, 7446-70-0; $[ReO_2(en)_2]^+$, 21602-78-8.

(41) (a) Miyata, S. *Clays Clay Miner.* **1975**, *23*, 369–375; **1983**, *31*, 305–311. (b) Miyata, S.; Okada, A. *Clays Clay Miner.* **1977**, *25*, 14–18. (c) Miyata, S.; Hirose, T. *Clays Clay Miner.* **1978**, *26*, 441–447.